View Article Online / Journal Homepage / Table of Contents for this issue
Dynamic Article Links

Journal of Materials Chemistry

Cite this: J. Mater. Chem., 2012, 22, 17055

www.rsc.org/materials

PAPER

Cu_2O/ZnO hetero-nanobrush: hierarchical assembly, field emission and photocatalytic properties†

Meenal Deo,[a] Deodatta Shinde,[b] Ashish Yengantiwar,[b] Jyoti Jog,[a] Beatrice Hannoyer,[c] Xavier Sauvage,[c] Mahendra More[b] and Satishchandra Ogale*[a]

Received 27th April 2012, Accepted 2nd July 2012
DOI: 10.1039/c2jm32660d

Zinc oxide (ZnO) nanorods are grown hierarchically on cuprous oxide (Cu_2O) nanoneedles to form a Cu_2O/ZnO hetero-nanobrush assembly. This increases the overall aspect ratio, which helps to enhance the field emission properties of the system. Also, the charge separation and transport are facilitated because of the multiple p–n junctions formed at p-Cu_2O/n-ZnO interfaces and quasi-1-D structures of both the materials, respectively. This helps to significantly enhance the photocatalytic properties. As compared to only Cu_2O nanoneedles, the Cu_2O/ZnO hetero-nanobrush shows excellent improvement in both field emission and photocatalytic applications.

Published on 03 July 2012. Downloaded by Pennsylvania State University on 06/03/2016 07:07:43.

Introduction

Since the discovery of carbon nanotubes,[1] quasi-1-D nanostructures have become an interesting and special class of materials because of their unique properties such as the specific nature of the electronic density of states, the possibility of ballistic charge transport, localization effects, increased surface area enabling surface electronic functionalization, *etc.* These lead to many applications in the field of electronics and opto-electronics.[2,3] Forming a branched 3-D structure of 1-D systems enhances the application domain even further. Indeed, such branched 3-D structures have found applications in the fields of solar energy conversion,[4] field electron emission,[5–8] gas sensing,[9] and photocatalysis.[10] ZnO is perhaps the most studied material in this respect because it can be easily formed into interesting 3-D morphologies by seeded secondary growth.[11] Interestingly, formation of heterostructures with components having different functionalities with favourable band alignment can not only lead to a functional integration of the properties of both the materials but also to novel interface effects and phenomena.[12] For example, some nanocomposites involving carbon nanostructures have shown excellent enhancement in photocatalytic activity over their components.[13,14] Semiconducting oxides are a special class of materials known for their broad range of electronic and optical properties and have therefore attracted scientific attention for recent years. Heterostructures of such metal oxides have been of significant interest in the context of diverse applications.[15] 3-D branched heterostructures in particular are now beginning to attract more attention due to the major advantages of tremendously increased surface area, enhanced heterojunction density, and intrinsic light harvesting effects. Various 3-D branched heterostructures of metal oxides have been pursued for different applications: For example, ZnO–WO_3,[16] SnO_2–WO_3 for field emission,[17] SnO_2–Fe_2O_3 for photocatalysis,[18] In_2O_3–SnO_2 for gas sensing,[19] Fe_2O_3–SnO_2 for Li-ion batteries,[20] and ternary oxides such as $MnMoO_4$–$CoMoO_4$ for supercapacitors.[21]

Cuprous oxide (Cu_2O) is one of the few p-type direct band gap metal oxide-based semiconductors (band gap ~2.17 eV). It has additional advantages of non-toxicity, low cost and abundance of its starting material, *i.e.* copper. Cu_2O has attracted interest as a good candidate material for solar cells,[22] photocatalysis,[23] and photo-electrochemical (PEC) water splitting[24] because of its favourable absorption in the visible range. However Cu_2O is far less explored in heterostructure nanomaterial form for various applications. It is also less explored for field electron emission studies although its work function (4.8 eV) is low. To our knowledge there are only two reports, one on a thin film form[25] and one on nanostructured Cu_2O[26] for field emission. ZnO is another interesting material which has n-type conductivity with a band gap of ~3.37 eV. It has been well studied for solar cell[27] and field emission[28] applications. The major advantage of ZnO is that it can be fabricated in various morphologies which are useful in different applications. Although a few heterojunction forms of Cu_2O/ZnO have been studied for photovoltaic[29–33] and photocatalytic[34–36] applications, clearly further work on the heterostructures of Cu_2O and ZnO is needed for enhanced functionality. In this paper, we report synthesis of the hetero-nanobrush comprising of Cu_2O nanoneedles decorated with ZnO

[a]*National Chemical Laboratory (NCL-CSIR), Dr Homi Bhabha Road, Pune, India, and Network Institute of Solar Energy (SCIR-NISE), New Dehli, India. E-mail: sb.ogale@ncl.res.in; Fax: +91 20 2590 2636; Tel: +91 20 2590 2260*
[b]*Center for Advanced Studies in Materials Science and Condensed Matter Physics, Department of Physics, University of PunePune, India*
[c]*University of Rouen, Groupe de Physique des Matériaux, CNRS-UMR 6634, BP-12, 76801 Saint Etienne du Rouvray Cedex, France*
† Electronic supplementary information (ESI) available. See DOI: 10.1039/c2jm32660d

View Article Online

Published on 03 July 2012. Downloaded by Pennsylvania State University on 06/03/2016 07:07:43.

nanorods by a two step chemical method. We have examined such a hetero-nanobrush system for field electron emission and photocatalysis applications.

Experimental section

Synthesis of Cu_2O/ZnO hetero-nanobrush on copper

The Cu_2O nanoneedle film was grown directly on copper substrate employing a protocol previously reported by us.[37] Copper foil was anodized in the presence of 2 M KOH which acts as electrolyte and graphite rod as the counter electrode. This leads to an evenly spread $Cu(OH)_2$ nanoneedle film on the Cu substrate, which on annealing at 450 °C in controlled oxygen pressure (5×10^{-6} mbar) gets converted into Cu_2O nanoneedles.

We carried out seed-assisted growth of ZnO on Cu_2O to achieve brush-like ZnO morphology. Thus a seed layer of ZnO was deposited by Pulsed Laser Deposition (PLD) technique on the Cu_2O nanoneedle film. The deposition was carried out in an oxygen pressure of 1×10^{-4} mbar at the substrate temperature of 100 °C for better adherence of the ultrathin ZnO surface nanostructure. For facile growth of ZnO on the seeded surface of Cu_2O, an equimolar (25 mM) solution of $Zn(NO_3)_2$ and hexamethylene tetramine (HMT) was used for the reaction. The reaction was carried out at 95 °C while stirring simultaneously for only 15 minutes. The samples were then rinsed with deionized water and dried in air. The Cu_2O/ZnO heterostructure films were then annealed in vacuum (5×10^{-5} mbar) at 250 °C for better adherence and better crystallinity of the nanostructure. This growth procedure is schematically shown in Fig. 1. From the high resolution SEM shown in Fig. 1(b), there are ZnO nanoparticles formed all over the surface of the Cu_2O nanoneedles by PLD, which ensures further growth of ZnO nanorods. The ZnO nanorod growth was carried out in the presence of hexamethylene tetramine (HMT) which covers non-polar surfaces of ZnO, other than the (002) plane system, to enhance the nanorod growth in the direction of (002). Fig. 1(c) gives the schematic and SEM image of the growth of ZnO nanorods on the surface of the Cu_2O nanoneedles. These heterostructured films were further characterized by using XRD, SEM and TEM.

General characterizations

Various techniques such as X-ray diffraction (XRD, Philips X'Pert PRO), Field Emission Scanning Electron Microscopy (FE-SEM, Hitachi S4800), UV-Vis spectro-photometer (Jasco V-570) were used for characterizations. The analytical transmission electron microscopy (TEM) was also performed with a probe-corrected ARM200F JEOL microscope operated at 200 kV. Energy Dispersive X-ray Spectroscopy (EDS) was performed with a JEOL JED2300 detector with a probe size of 0.2 nm.

Field emission and photocatalysis experiments

The field emission (FE) current density–electric field (*J–E*) characteristic measurements were carried in all-metal field emission microscope with a load lock chamber. The FE studies were carried out in a planar diode configuration, wherein Cu_2O nanoneedles or Cu_2O/ZnO hetero-nanobrushes served as a cathode and a semi-transparent cathodoluminescent phosphor screen (ZnS : Cu Green Color) as an anode. The cathode was pasted onto a sample holder using vacuum compatible conducting silver paste and was held in front of the anode screen at a distance of ~500 μm. The emission current density–applied

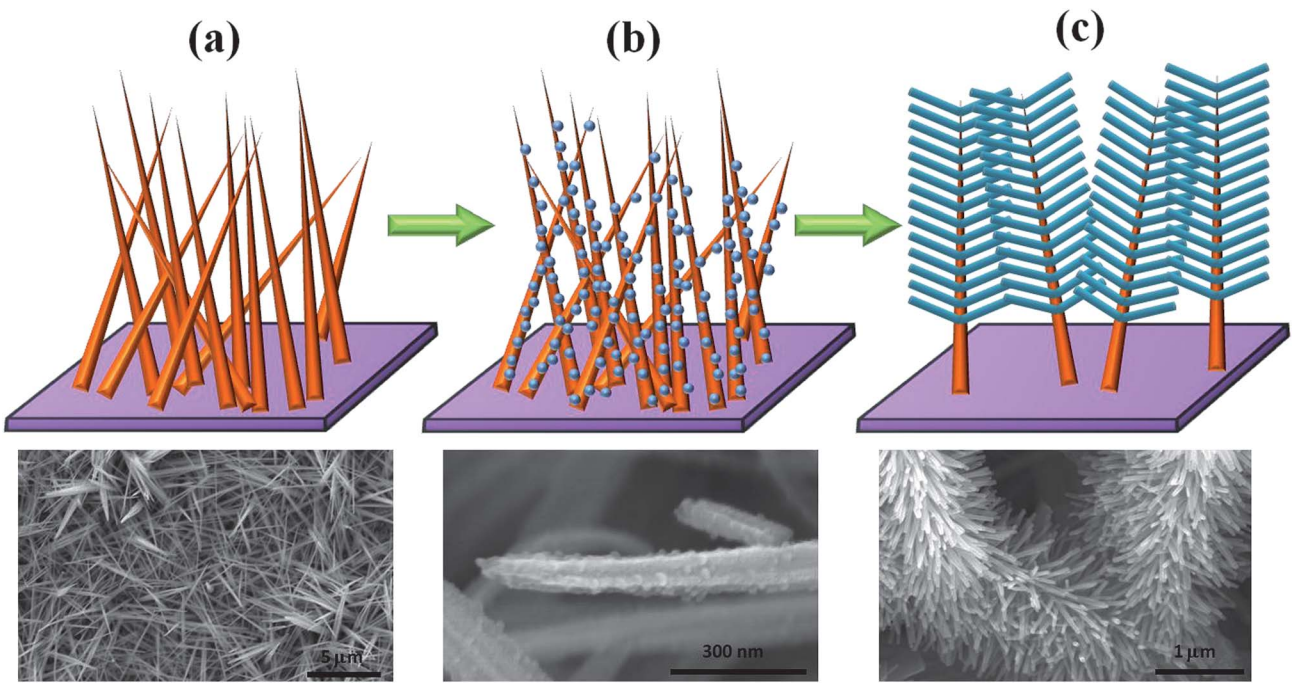

Fig. 1 Schematic of the growth procedure of Cu_2O/ZnO hetero-nanobrush. The bottom pictures show SEM images of each growth step.

 This journal is © The Royal Society of Chemistry 2012

View Article Online

Published on 03 July 2012. Downloaded by Pennsylvania State University on 06/03/2016 07:07:43.

electric field (*J–E*) characteristic measurements were carried out at 1×10^{-8} mbar pressure using a Keithley 6514 electrometer and a Spellman high-voltage DC power supply (0–40 kV). For FE, we kept the area of the specimen at 1 cm^2.

The photocatalysis measurements were done at room temperature and in 10^{-5} M aqueous solution of methyl orange (MO), used as a pollutant. The Cu_2O nanoneedles and Cu_2O/ZnO heterostructure films of the same area were directly dipped into the methyl orange solution. The solution was first stirred in the dark in the presence of the film for 30 minutes before photocatalytic measurements so as to reach the adsorption–desorption equilibrium. Then it was continuously stirred under solar simulator (AM 1.5, 100 mW cm^{-2}) used for illumination. The spectral intensity distribution was analyzed using UV-Vis spectro-photometer for specific intervals of time for a total time of 2.5 hours.

Results and discussion

Characterization of Cu_2O/ZnO heterostructure

The morphology of the as-synthesized Cu_2O/ZnO heterostructure was imaged by Field Emission Scanning Electron Microscopy (FESEM). Fig. 2(a) shows the low magnification SEM image, which reveals a uniform formation of brush-like structures. From the high magnification SEM images, shown in the inset of Fig. 2(a), it is seen that ZnO nanorods have been decorated all over the Cu_2O nanoneedle surface forming the hetero-nanobrush morphology. It is also seen that the length of a single ZnO nanorod is around 500 nm with a hexagonal cross section having a diameter about 50 nm.

Fig. 2(b) shows the X-Ray Diffraction (XRD) pattern of Cu_2O/ZnO hetero-nanobrush. The XRD shows a polycrystalline phase of Cu_2O nanoneedles grown directly on copper. The formation of the ZnO phase is also confirmed by XRD. During the deposition of ZnO nanorods on these Cu_2O nanoneedles, even if the deposition is carried out at 95 °C in air, the Cu_2O phase does not get converted into CuO. This can be attributed to uniform growth and surface coverage of the ZnO seed layer by PLD, which also acts as a protecting layer for Cu_2O avoiding its further oxidation.

To reveal the precise morphology and the interconnection of the two phases detected by XRD (namely Cu_2O and ZnO), some TEM observations were carried out. As shown in Fig. 3(a), the structure of the hetero-nanobrushes consists of a core nanoneedle covered by nanorods that are seen to nucleate and grow on its surface. EDS elemental mapping (Fig. 3(b), (d) and (e)), clearly brings out the copper-rich core and the Zn-rich shell. SAED patterns recorded on the nanoneedle (Fig. 3(c)) and on the nanorod (Fig. 3(f)) confirm that the two pure phases present are Cu_2O and ZnO, respectively, in agreement with the XRD data. The typical diameter of ZnO nanorods measured from TEM images is in a range of 30 to 50 nm, while the mean diameter of Cu_2O nanoneedles is about 100 nm. Using EDS analysis, the composition of both oxides was qualitatively estimated. A Zn : O (Cu : O) ratio of 0.96 (1.94) was found for the ZnO (Cu_2O), in good agreement with the expected stoichiometry. We have performed HRTEM analysis of Cu_2O nanoneedle and ZnO nanorods grown on Cu_2O nanoneedles to find exact crystal growth directions of both Cu_2O and ZnO, as shown in Fig. 4(a) and (b), respectively. We find that Cu_2O nanoneedle grows along [220] direction, while the ZnO nanorods grow along the [002] direction. As the growth direction of hexagonal ZnO nanorods is along [002], the six surface facets of ZnO nanorods are along the $(10\bar{1}0)$ family of planes which are perpendicular to the [002] direction. The Cu_2O surface facets, which are found from HRTEM analysis, are mostly along (111) planes.

Field emission studies

The field emission properties of Cu_2O are rarely studied, in contrast to the other semiconducting oxides such as ZnO, SnO_2, WO_3, *etc.* Moreover the possibility of the enhancement in its field emission properties by making its composites with other materials has not been explored yet. We have therefore studied the

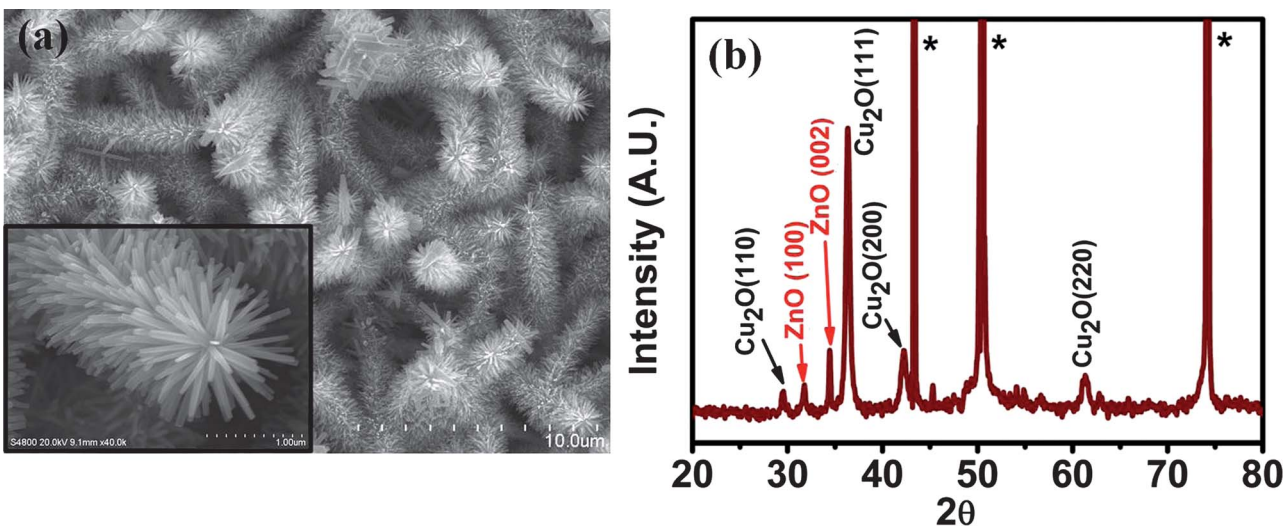

Fig. 2 (a) Low-magnification FESEM image of Cu_2O/ZnO hetero-nanobrush; inset shows high-magnification FESEM image. (b) X-Ray diffraction pattern of Cu_2O/ZnO hetero-nanobrush. * represent copper substrate peaks.

View Article Online

Published on 03 July 2012. Downloaded by Pennsylvania State University on 06/03/2016 07:07:43.

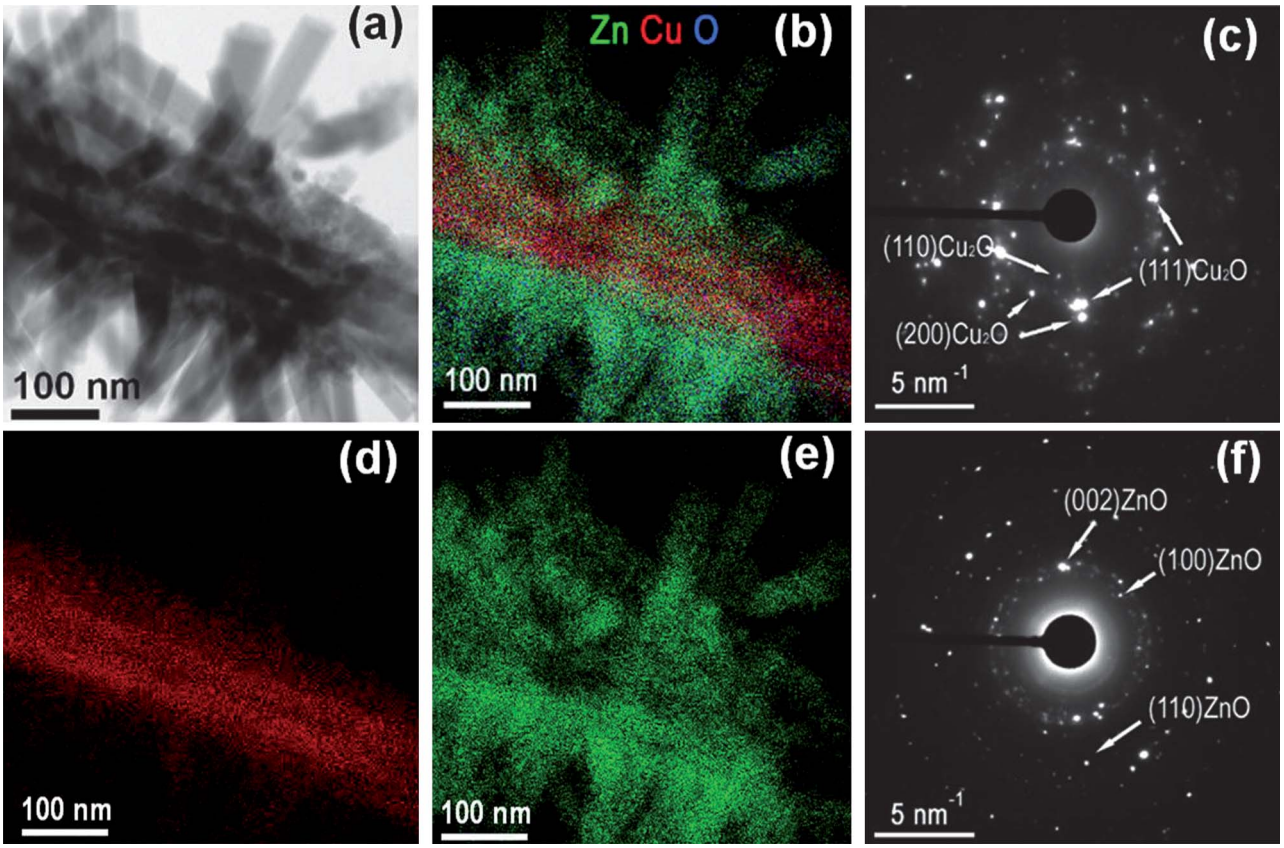

Fig. 3 (a) Bright field STEM image of a Cu_2O/ZnO hetero-nanobrush and (b) corresponding EDS elemental mapping showing the distribution of Zn (green), Cu (red) and O (blue) within the structure, and separate elemental mapping of (d) Cu and (e) Zn; SAED pattern obtained with a small probe located on the (c) cuprous oxide nano-needle and (f) on the zinc oxide nanorods, confirming that only two phases are present, namely Cu_2O and ZnO.

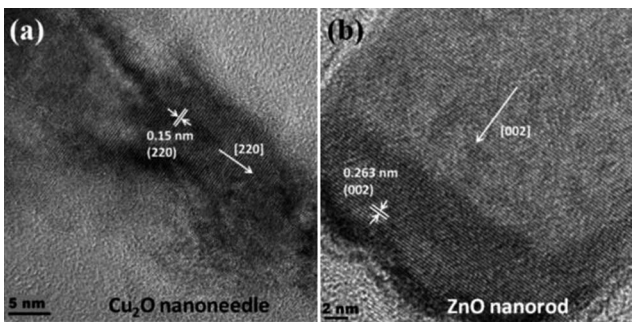

Fig. 4 HRTEM images of (a) Cu_2O nanoneedle and (b) ZnO nanorod.

field emission properties of Cu_2O nanoneedles and also Cu_2O/ZnO hetero-nanobrushes.

Fig. 5(a) depicts the field emission current density as a function of the applied electric field (*J*–*E*) plot. The turn-on field and threshold field, defined respectively as the fields required to draw an emission current density of ~10 μA cm^{-2} and ~100 μA cm^{-2}, are found to be ~8.4 V μm^{-1} and ~11.8 V μm^{-1} respectively for Cu_2O nanoneedles, and ~6.5 V μm^{-1} and ~8.9 V μm^{-1} respectively for the Cu_2O/ZnO nanobrush sample. The relatively lower turn-on field for the Cu_2O/ZnO heterostructure can be attributed to its unique geometrical form (which controls the field distribution) along with favourable band structure. As reported by Ujjal Gautam *et al.*,[38] in the case of such branched structures, the applied primary field gets enhanced at the stems (Cu_2O nanoneedles in our case) which successively act as a secondary field for the branches (ZnO nanorods in our case), thereby enhancing the local electric field.

Interestingly, the current density in the case of the Cu_2O/ZnO nanobrush is seen to have increased dramatically to ~425 μA cm^{-2} in comparison to ~40 μA cm^{-2} in the case of Cu_2O nanoneedles at an applied electric field of ~10.5 V μm^{-1}. This tremendous increase in the current density can be attributed to the branched structure, which acts as multiple emitters. As reflected from the basics of field emission, the emission current density is mainly decided by the intrinsic property (work function) and the extrinsic property (shape and size) of the emitter material. Thus for a better field emission performance the material with low work function should be in quasi-1-D form and preferably oriented perpendicular to the substrate *i.e.* vertically aligned. As seen from the SEM image (Fig. 1(a)), the random orientation of the Cu_2O nanoneedles is also responsible for their inferior FE characteristics as compared to Cu_2O/ZnO hetero-nanobrushes. On the other hand, in case of Cu_2O/ZnO nanobrush (Fig. 2(a)) there are relatively fair number of emitters pointing towards the anode; thus the effective electric field experienced by an individual ZnO nanorod will be more compared to only an Cu_2O nanoneedle and hence enhancement in the field emission current is observed.

 This journal is © The Royal Society of Chemistry 2012

View Article Online

Published on 03 July 2012. Downloaded by Pennsylvania State University on 06/03/2016 07:07:43.

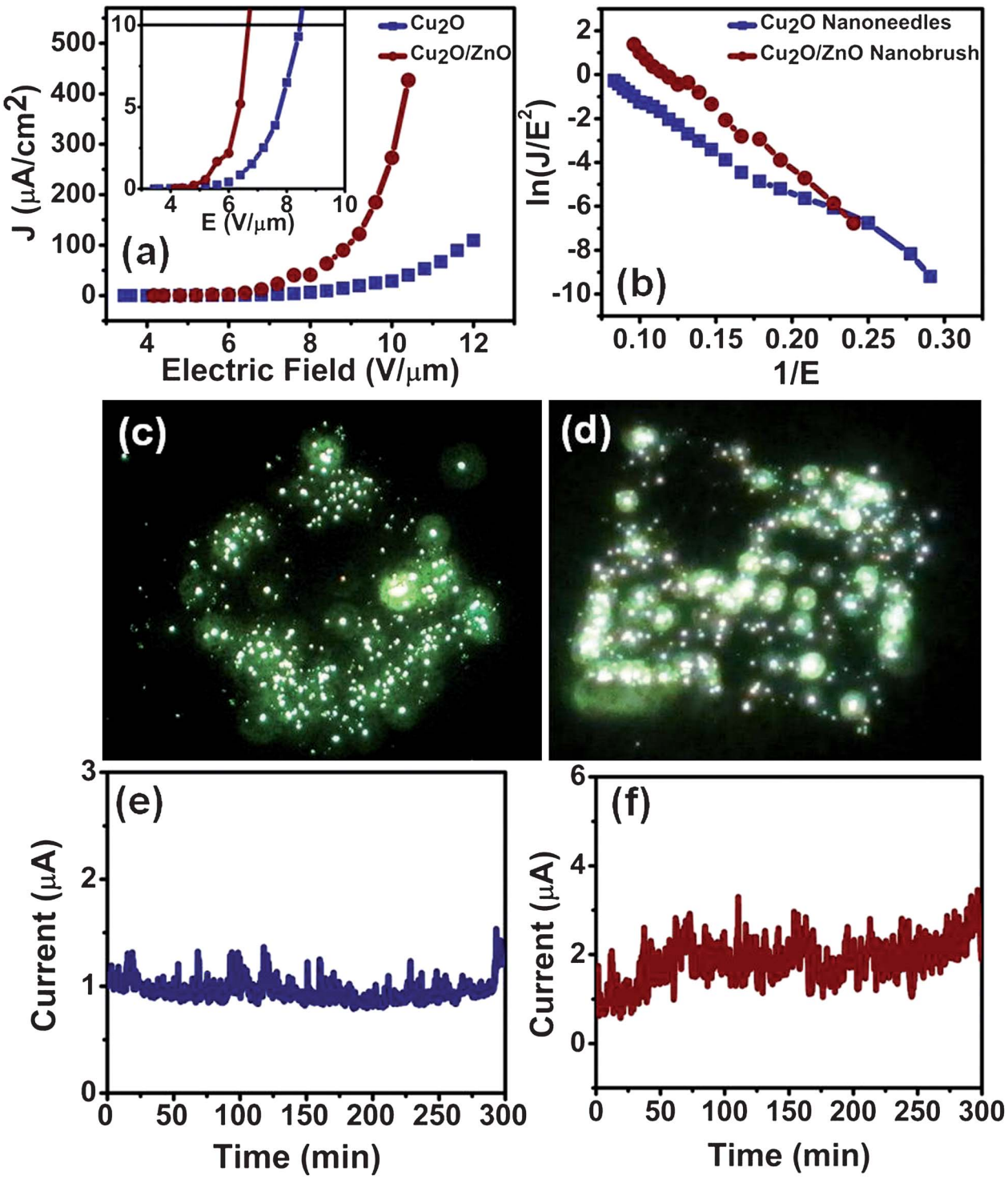

Fig. 5 (a) Field emission current density–applied electric field (*J*–*E*) characteristics (inset shows turn-on value); (b) corresponding Fowler–Nordheim (F–N) plot of Cu_2O nanoneedles and Cu_2O/ZnO nanobrush; (c) and (d) show the field emission micrographs of Cu_2O nanoneedles and Cu_2O/ZnO nanobrush, respectively. The traces in (e) and (f) show the current stability for Cu_2O nanoneedles and Cu_2O/ZnO nanobrush, respectively.

This phenomenon can be further discussed on the basis of the band diagram of Cu_2O/ZnO heterostucture schematically shown in Fig. 6. Normally in the case of the field emission from heterostructures, it is well accepted that the work function of the shell material should be lower than that of the core material.

Considering the work functions of Cu_2O and ZnO of about 4.8 eV and 5.3 eV, respectively, one could expect a higher value of the turn-on field in the case of Cu_2O/ZnO nanobrushes than that of only Cu_2O nanoneedles. But, when these two materials come into contact, there is formation of a p–n junction at their

View Article Online

Published on 03 July 2012. Downloaded by Pennsylvania State University on 06/03/2016 07:07:43.

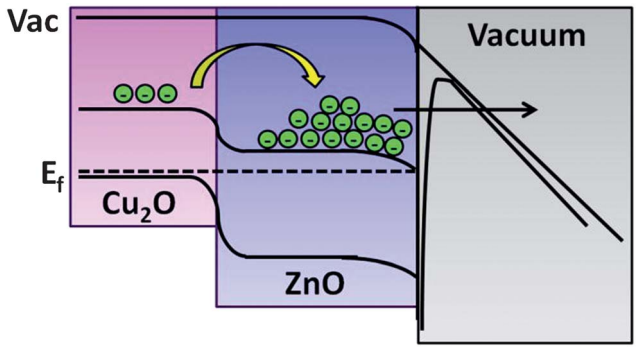

Fig. 6 Band diagram of Cu_2O/ZnO heterojunction.

interface and there is a favourable band alignment for the electron transport from the conduction band of core Cu_2O to the conduction band of shell ZnO, as shown in Fig. 6.

In any practical measurement, the turn-on field is defined as the field at which the emission current attains a specific chosen value. It is taken as 10 μA cm^{-2} in our case, as in many other works. This value then also depends on the number of emission points (tips) per cm^2 in addition to the value of the work function. In the present case, since a number of ZnO brush-like strands grow on each Cu_2O tip, the density of emission points is considerably higher in the case of ZnO/Cu_2O hetero-brush, as clear from SEM images shown in the ESI.† Hence, in spite of the higher work function of ZnO, the current density of 10 μA cm^{-2} is reached at a lower applied field. Thus the effective turn-on field is lower.

The field emission characteristics were further analysed by Fowler–Nordheim equation,[39] which is given by:

$$J = \left(\frac{A\beta^2E^2}{\varphi}\right)\exp\left(-\frac{B\,\varphi^{3/2}}{\beta E}\right)$$

where $A = 1.54 \times 10^{-6}$ A eV V^{-2} and $B = 6.83 \times 10^3$ $eV^{-3/2}$ V μm^{-1}, J is the current density, E is the applied electric field, φ is the work function of emitting material and β is field enhancement factor.

The Fowler–Nordheim (F–N) plot derived from the observed J–E characteristic is shown in Fig. 5(b). The F–N plot shows an overall linear behaviour with decrease in the slope (non-linearity) at very high applied field range. Such a type of F–N plot exhibiting a tendency toward nonlinearity at very high applied field has been also reported in our previous work.[17]

The field emission micrographs corresponding to Cu_2O nanoneedles and Cu_2O/ZnO nanobrush emitters are shown in Fig. 5(c) and (d), respectively. The number of spots for the Cu_2O/ZnO nanobrush is larger because of the increased density of the emission sites as compared to Cu_2O nanoneedles. More non-uniformity of the emission spots in case Cu_2O also suggests that all the needles cannot take part in the emission at lower applied fields.

For field emission electron sources, along with the emission competence, the current stability is also a decisive and important parameter. The current stability curve (I–t plot) recorded for Cu_2O nanoneedles is shown in Fig. 5(e), which shows that the emission current is quite steady, whereas an instability in the emission current is seen for Cu_2O/ZnO nanobrush (Fig. 5(f)). This can be attributed to the adsorption–desorption of residual gas molecules present in the ambient of the specimen. The instability in emission current in Cu_2O/ZnO nanobrush can be attributed to the densely crowded ZnO branches which cause more surface area for the adsorption and diffusion of residual gas molecules on the emitter surface. Other considerations, such as field migration of oxygen vacancies, mild ion bombardment, *etc.*, may also be operative.

Photocatalysis

In view of the favourable band alignment of Cu_2O and ZnO for efficient separation of charges, we studied the photocatalytic activity of Cu_2O nanoneedles and Cu_2O/ZnO hetero-nanobrushes for degradation of methyl orange (MO) dye in the presence of simulated sunlight, as shown respectively in Fig. 7(a) and (b).

The Cu_2O nanoneedle film and Cu_2O/ZnO nanobrush film were treated in the dark for 30 minutes before the photocatalytic measurements (light on) to eliminate the possibility that higher adsorption site density in the case of the Cu_2O/ZnO nanobrush did not simply adsorb more dye molecules and hence showed an "apparent" rapid dye removal from the solution that is examined optically. It can be clearly seen from Fig. 7(a) and (b) that there is hardly any change in the intensity of MO after 30 minutes treatment in the dark. Also, from Fig. 7(a) and (b) we can notice that the Cu_2O/ZnO nanobrush system can degrade the dye almost completely in 120 minutes under illumination, which is not possible with the Cu_2O nanoneedles alone. By considering the intensity of measured peak of methyl orange at 464 nm, we have plotted the corresponding rates of degradation by Cu_2O and Cu_2O/ZnO, as shown in Fig. 7(c), which indicates that the rate in the presence of Cu_2O/ZnO is much faster than only Cu_2O. According to this data, after 2 hours in the presence of light, the amount of MO remaining in the case of Cu_2O nanoneedles is around 70% while that in the case of Cu_2O/ZnO nanobrush is only around 7%.

There can be two possible reasons for this fast photocatalysis in the case of Cu_2O/ZnO. Because of the special brush-like morphology, the surface area in the case of Cu_2O/ZnO nanobrush is much greater than that of Cu_2O nanoneedles which is highly advantageous for good photocatalytic activity.[40] Also, the Cu_2O is p-type, having a band gap of 2.1 eV, which absorbs visible light, but there is a possibility of recombination in the case of only Cu_2O. When we make Cu_2O/ZnO heterostructures there is a favourable p–n junction formation which helps in the separation of the generated electron–hole pairs in the presence of light and avoids recombination. This is shown schematically in Fig. 7(d). Also, because of the quasi-1-D nature of both Cu_2O and ZnO, the generated charges can very quickly come to the surface, which contributes to the degradation of dye. After the separation of electrons and holes, there are some reactions involved for the formation of $\dot{O}H$ radicals, which can be written as:[41]

$$h^+ + H_2O \rightarrow H^+ + \dot{O}H$$

$$e^- + O_2 \rightarrow \dot{O}_2^-$$

$$\dot{O}_2^- + H^+ \rightarrow HO_2^{\cdot}$$

 This journal is © The Royal Society of Chemistry 2012

View Article Online

Published on 03 July 2012. Downloaded by Pennsylvania State University on 06/03/2016 07:07:43.

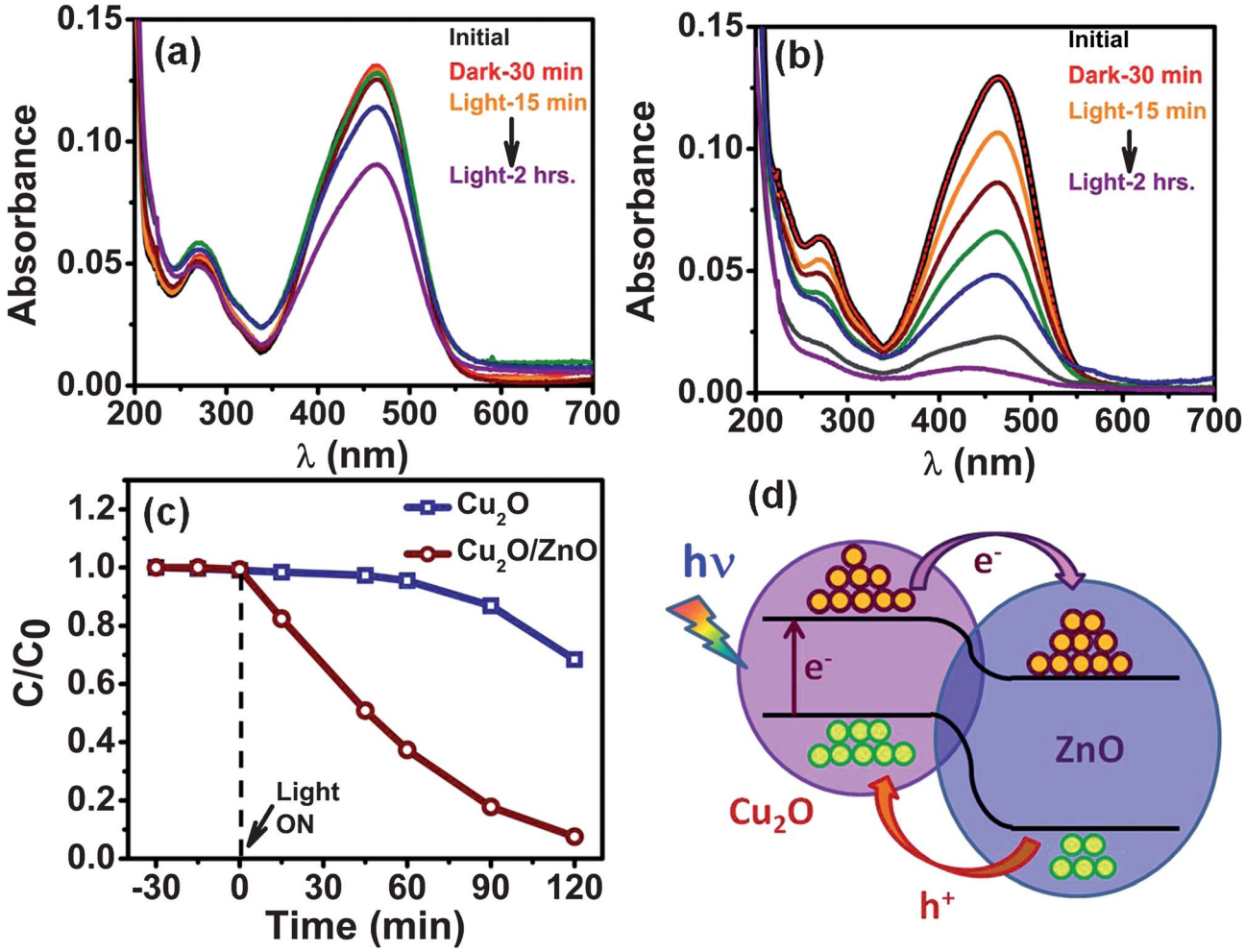

Fig. 7 UV-Vis absorption spectroscopy of methyl orange dye taken at different times under visible light in the presence of (a) Cu_2O nanoneedles and (b) Cu_2O/ZnO nanobrush; (c) rates of corresponding methyl orange degradation; (d) schematic diagram showing charge generation and transfer in the presence of light causing degradation of dye.

$$HO_2^{\cdot} + H^+ + {}^{\cdot}O_2^- \rightarrow H_2O_2 + O_2$$

$$H_2O_2 + e^- \rightarrow OH^{\cdot} + OH^-$$

These hydroxyl radicals are known to be very reactive oxidative species which react with the organic molecules or water pollutants and degrade them.

Conclusion

We have synthesized Cu_2O/ZnO hetero-nanobrush on copper substrate by a simple chemical route. The Cu_2O/ZnO hetero-nanobrush leads to the formation of multiple p–n junctions, and enhancement of the surface area and tip density. These properties are utilized in the applications of field electron emission and photocatalysis. We observe that for the Cu_2O/ZnO nanobrush case the field emission current increases and turn-on field decreases significantly in comparison to the case of Cu_2O nanoneedles. The Cu_2O/ZnO nanobrush structure is also shown to be a good candidate for photocatalysis as it degrades methyl orange effectively than only Cu_2O nanoneedles.

Acknowledgements

This work is supported by the Council of Scientific and Industrial Research (CSIR, Govt. of India) and University Grants Commission (UGC, India). MD would like to acknowledge fellowship support by CSIR. DS is thankful to DRDO, India and Director, MTRDC for financial support. Authors are thankful to Centre for Materials for Electronics Technology (C-MET), Pune for the FESEM facility. SBO acknowledges funding under the CSIR TAPSUN program.

References

1 S. Iijima, *Nature*, 1991, **354**, 56–58.
2 J. G. Lu, P. Chang and Z. Fan, *Mater. Sci. Eng., R*, 2006, **52**, 49–91.
3 T. Zhai, L. Li, Y. Ma, M. Liao, X. Wang, X. Fang, J. Yao, Y. Bando and D. Golberg, *Chem. Soc. Rev.*, 2011, **40**, 2986–3004.
4 M. J. Bierman and S. Jin, *Energy Environ. Sci.*, 2009, **2**, 1050–1059.
5 Z. Wang, J. Gong, Y. Su, Y. Jiang and S. Yang, *Cryst. Growth Des.*, 2010, **10**, 2455–2459.
6 C. Cao, Z. Chen, X. An and H. Zhu, *J. Phys. Chem. C*, 2008, **112**, 95–98.
7 Z.-G. Chen, L. Cheng, H.-Y. Xu, J.-Z. Liu, J. Zou, T. Sekiguchi, G. Q. Lu and H.-M. Cheng, *Adv. Mater.*, 2010, **22**, 2376–2380.

View Article Online

Published on 03 July 2012. Downloaded by Pennsylvania State University on 06/03/2016 07:07:43.

8 G. Li, T. Zhai, Y. Jiang, Y. Bando and D. Golberg, *J. Phys. Chem. C*, 2011, **115**, 9740–9745.
9 N. Zhang, K. Yu, Q. Li, Z. Q. Zhu and Q. Wan, *J. Appl. Phys.*, 2008, **103**, 104305.
10 C. Fang, B. Geng, J. Liu and F. Zhan, *Chem. Commun.*, 2009, 2350–2352.
11 S. H. Ko, D. Lee, H. W. Kang, K. H. Nam, J. Y. Yeo, S. J. Hong, C. P. Grigoropoulos and H. J. Sung, *Nano Lett.*, 2011, **11**, 666–671.
12 D. J. Milliron, S. M. Hughes, Y. Cui, L. Manna, J. Li, L.-W. Wang and A. P. Alivisatos, *Nature*, 2004, **430**, 190–195.
13 J. Du, X. Lai, N. Yang, J. Zhai, D. Kisailus, F. Su, D. Wang and L. Jiang, *ACS Nano*, 2011, **5**, 590–596.
14 S. Wang, L. Yi, J. E. Halpert, X. Lai, Y. Liu, H. Cao, R. Yu, D. Wang and Y. Li, *Small*, 2012, **8**, 265–271.
15 J. Hu, Y. Bando and D. Golberg, *J. Mater. Chem.*, 2009, **19**, 330–343.
16 H. Kim, S. Jeon, M. Lee, J. Lee and K. Yong, *J. Mater. Chem.*, 2011, **21**, 13458–13463.
17 D. R. Shinde, P. G. Chavan, S. Sen, D. S. Joag, M. A. More, S. C. Gadkari and S. K. Gupta, *ACS Appl. Mater. Interfaces*, 2011, **3**, 4730–4735.
18 M. Niu, F. Huang, L. Cui, P. Huang, Y. Yu and Y. Wang, *ACS Nano*, 2010, **4**, 681–688.
19 Y.-C. Her, C.-K. Chiang, S.-T. Jean and S.-L. Huang, *CrystEngComm*, 2012, **14**, 1296–1300.
20 W. Zhou, C. Cheng, J. Liu, Y. Y. Tay, J. Jiang, X. Jia, J. Zhang, H. Gong, H. H. Hng, T. Yu and H. J. Fan, *Adv. Funct. Mater.*, 2011, **21**, 2439–2445.
21 L.-Q. Mai, F. Yang, Y.-L. Zhao, X. Xu, L. Xu and Y.-Z. Luo, *Nat. Commun.*, 2011, **2**, 381.
22 B. P. Rai, *Sol. Cells*, 1988, **25**, 265–272.
23 Y. Zhang, B. Deng, T. Zhang, D. Gao and A.-W. Xu, *J. Phys. Chem. C*, 2010, **114**, 5073–5079.
24 A. Paracchino, V. Laporte, K. Sivula, M. Grätzel and E. Thimsen, *Nat. Mater.*, 2011, **10**, 456–461.
25 Q. Tang, T. Li, X. Chen, D. Yu and Y. Qian, *Solid State Commun.*, 2005, **134**, 229–231.
26 H. Shi, K. Yu, F. Sun and Z. Zhu, *CrystEngComm*, 2012, **14**, 278.
27 Q. Zhang, C. S. Dandeneau, X. Zhou and G. Cao, *Adv. Mater.*, 2009, **21**, 4087–4108.
28 G. Shen, Y. Bando, B. Liu, D. Golberg and C.-J. Lee, *Adv. Funct. Mater.*, 2006, **16**, 410–416.
29 B. D. Yuhas and P. Yang, *J. Am. Chem. Soc.*, 2009, **131**, 3756–3761.
30 J. Cui and U. J. Gibson, *J. Phys. Chem. C*, 2010, **114**, 6408–6412.
31 H. Wei, H. Gong, Y. Wang, X. Hu, L. Chen, H. Xu, P. Liu and B. Cao, *CrystEngComm*, 2011, **13**, 6065–6070.
32 K. P. Musselman, A. Marin, A. Wisnet, C. Scheu, J. L. MacManus-Driscoll and L. Schmidt-Mende, *Adv. Funct. Mater.*, 2011, **21**, 573–582.
33 T.-J. Hsueh, C.-L. Hsu, S.-J. Chang, P.-W. Guo, J.-H. Hsieh and I.-C. Chen, *Scr. Mater.*, 2007, **57**, 53–56.
34 C. Xu, L. Cao, G. Su, W. Liu, H. Liu, Y. Yu and X. Qu, *J. Hazard. Mater.*, 2010, **176**, 807–813.
35 Y. Wang, G. She, H. Xu, Y. Liu, L. Mu and W. Shi, *Mater. Lett.*, 2012, **67**, 110–112.
36 Q. Zhu, Y. Zhang, F. Zhou, F. Lv, Z. Ye, F. Fan and P. K. Chu, *Chem. Eng. J.*, 2011, **171**, 61–68.
37 M. Deo, S. Mujawar, O. Game, A. Yengantiwar, A. Banpurkar, S. Kulkarni, J. Jog and S. Ogale, *Nanoscale*, 2011, **3**, 4706.
38 U. K. Gautam, X. Fang, Y. Bando, J. Zhan and D. Golberg, *ACS Nano*, 2008, **2**, 1015–1021.
39 X. Fang, Y. Bando, U. K. Gautam, C. Ye and D. Golberg, *J. Mater. Chem.*, 2008, **18**, 509–522.
40 F. Lu, W. Cai and Y. Zhang, *Adv. Funct. Mater.*, 2008, **18**, 1047–1056.
41 K.-i. Okamoto, Y. Yamamoto, H. Tanaka, M. Tanaka and A. Itaya, *Bull. Chem. Soc. Jpn.*, 1985, **58**, 2015–2022.

 This journal is © The Royal Society of Chemistry 2012